

Quasi-One-Dimensional Fermi Surface Nesting and Hidden Nesting Enable Multiple Kohn Anomalies in α -Uranium

Aditya Prasad Roy,¹ Naini Bajaj,¹ Ranjan Mittal^{2,4}, Peram D. Babu³, and Dipanshu Bansal^{1*}

¹Department of Mechanical Engineering, Indian Institute of Technology Bombay, Mumbai, MH 400076, India

²Solid State Physics Division, Bhabha Atomic Research Centre, Mumbai, MH 400085, India

³UGC-DAE Consortium for Scientific Research, Mumbai Centre, R5-Shed, BARC, Trombay, Mumbai, MH 400085, India

⁴Homi Bhabha National Institute, Anushaktinagar, Mumbai, MH 400094, India



(Received 2 August 2020; revised 20 January 2021; accepted 22 January 2021; published 1 March 2021)

The topology of the Fermi surface controls the electronic response of a metal, including charge density wave (CDW) formation. A topology conducive for Fermi surface nesting (FSN) allows the electronic susceptibility χ_0 to diverge and induce a CDW at wave vector \mathbf{q}_{CDW} . Kohn extended the implications of FSN to show that the imaginary part of the lattice dynamical susceptibility χ_L'' also responds anomalously for all phonon branches at \mathbf{q}_{CDW} —a phenomenon referred to as the Kohn anomaly. However, materials exhibiting multiple Kohn anomalies remain rare. Using first-principles simulations of χ_0 and χ_L'' , and previous scattering measurements [Crummett *et al.*, Phys. Rev. B **19**, 6028–234 (1979)], we show that α -uranium harbors multiple Kohn anomalies enabled by the combined effect of FSN and “hidden” nesting, i.e., nesting of electronic states above and below the Fermi surface. FSN and hidden nesting lead to a *ridgelike* feature in the real part of χ_0 , allowing interatomic forces to modulate strongly and multiple Kohn anomalies to emerge. These results emphasize the importance of hidden nesting in controlling χ_0 and χ_L'' to exploit electronic and lattice states and enable engineering of advanced materials, including topological Weyl semimetals and superconductors.

DOI: [10.1103/PhysRevLett.126.096401](https://doi.org/10.1103/PhysRevLett.126.096401)

In the Peierls description of a charge density wave (CDW), an ideal one-dimensional (1D) chain is electronically unstable [1,2]. Fermi surface nesting (FSN) in a 1D chain leads to the divergence of the imaginary part of the electronic susceptibility, i.e., $\text{Im}\{\chi_0(\mathbf{q}, \omega = 0)\}$, at $|\mathbf{q}_{\text{CDW}}| = 2k_F = \pm\pi/a$, which is carried over to the real part $\text{Re}\{\chi_0(\mathbf{q})\}$ [3–6]. The divergence of $\text{Re}\{\chi_0(\mathbf{q})\}$ governs the electronic instability [5]. Here \mathbf{q} is the wave vector, ω is the frequency, k_F is the magnitude of the Fermi wave vector, and a is the lattice constant. For brevity, we omit ω from $\chi_0(\mathbf{q}, \omega)$ when it is zero. Kohn extended the idea of electronic instability to the lattice and showed that the divergence of the derivative of $F(\mathbf{q}) \propto \text{Re}\{\chi_0(\mathbf{q})\}/|\mathbf{q}|^2$ [see Eqs. (4)–(6) of Ref. [7]] abruptly decreases the ability of electrons to screen an embedded charge distribution for $|\mathbf{q}| > 2k_F$. This change in screening strongly modulates the interatomic forces F_{ij} , thus inducing Kohn anomalies $[\nabla_{\mathbf{q}}\omega(\mathbf{q}) \rightarrow \infty]$ in *all* the phonon branches at $|\mathbf{q}| = 2k_F$ (except for symmetry forbidden branches). Nevertheless, as mentioned by Johannes and Mazin [5], experimentally, such an observation remains rare.

Several arguments could be put forward for the rare nature of this phenomenon. One which has sound experimental and theoretical evidence is the *wavevector-dependent* electron-phonon interaction (EPI) [6,8–15] mechanism of CDW formation, where an electron scatters to another state by absorption or emission of a phonon.

The energy and momentum of the electron-phonon (e -ph) system are conserved [16,17]. However, severe restrictions are imposed on the e -ph scattering phase space by a fixed \mathbf{q}_{CDW} [17], and conservation is unlikely to be satisfied for all phonon branches simultaneously. Hence, we do not observe a Kohn anomaly or a peak (or kink) in phonon linewidths (Γ_{LW}) for all branches at \mathbf{q}_{CDW} as, for example, seen in NbSe₂ [8,9], TbTe₃ [11], and DyTe₃ [12]. Other arguments for the observed rarity relate to the material’s Fermi surface or instrumental issues like finite energy and momentum resolution of inelastic scattering experiments. In general, FSN is far from perfect due to finite temperature effects and the lifetime of coupled electron quasiparticles, thus suppressing the divergence of $\text{Re}\{\chi_0(\mathbf{q})\}$ [5]. Consequently, with an ill-defined FSN wave vector, a Kohn anomaly is less prone to be observable for all phonon branches at \mathbf{q}_{CDW} . Moreover, the nesting wave vector is generally localized in reciprocal lattice, so is the corresponding Kohn anomaly [1–3,18,19]. Because of the finite momentum transfer (i.e., \mathbf{Q}) resolution volume in experiments (x ray or neutron), a localized Kohn anomaly is smeared out and not easily observable.

Hence, for conclusive evidence of a Kohn anomaly in multiple phonon branches at \mathbf{q}_{CDW} above the CDW transition, the FSN must be perfect for an entire reciprocal lattice plane or at least for a significant part of it, rather than being localized to a single wave vector. However, such a system is

challenging to realize. Using comprehensive first-principles simulations supported by previous scattering experiments [20], we find α -uranium (hereafter referred to as α -U) harbors a CDW and multiple Kohn anomalies at \mathbf{q}_{CDW} . We explicitly demonstrate that despite imperfect FSN (where only a few parts of the reciprocal lattice contribute), the combined effect of avoided band crossings and hidden nesting facilitated by favorable Fermi surface velocity drives the electronic instability and the CDW state. Importantly, we find $\text{Re}\{\chi_0(\mathbf{q})\}$ is delocalized in the reciprocal lattice and has a (quasi-)1D response. Consequently, the induced lattice response $\chi_L''(\mathbf{Q}, E = \hbar\omega)$ is also (quasi-)1D. This 1D lattice response enables experimental observation of the weak and strong Kohn anomalies in multiple phonon branches at \mathbf{q}_{CDW} , not limited by finite \mathbf{Q} resolution. This unique behavior of α -U was not recognized in previous experimental and computational studies, which primarily focused on weakly correlated f -electron states near the Fermi energy [21–25], CDW phase transition [20,26,27], and temperature- or pressure-dependent (an)harmonic response and EPI [28–31].

Structural distortion and CDW transition.—Below the melting point of $T_M \simeq 1405$ K, uranium crystallizes in a body-centered cubic γ -U phase, and undergoes structural phase transitions from γ -U to the tetragonal β -U phase at 1045 K, and β -U to the orthorhombic α -U phase at 935 K [27,32]. The α -U phase ($Cmcm$, space group no. 63)—the phase of interest for the present study—remains stable down to $T_{\text{CDW}} \sim 43$ K, confirmed also by our *ab initio*

molecular dynamics (AIMD) simulations [Figs. 1(a) and 1(c)]. For $T < T_{\text{CDW}}$, the electronic instability drives the CDW transition to the α_1 -U phase, as we show later. A peak corresponding to the CDW transition appears in the total heat capacity (C_p) measurements on both single-crystal [33] and polycrystalline [34] samples (Supplemental Material, Fig. S1c [35]). The CDW wave vector $\mathbf{q}_{\text{CDW}} = (q_x, q_y, q_z)$ continues to change on cooling within the α_1 -U phase (Supplemental Material, Figs. S1a and S1b). At $T = T_{\alpha_{12}} \sim 37$ K, q_x locks in at 0.5 r.l.u. [64,65], and the unit cell is doubled along the a axis leading to the α_2 -U phase [Figs. 1(c) and 1(d)]. Here r.l.u. refers to reciprocal lattice units. The hysteresis in x-ray [65] and neutron [64] diffraction and C_p [33] measurements found the transition at $T_{\alpha_{12}}$ to be first order (not shown here). Notably, the peak in C_p at $T_{\alpha_{12}}$ is only observed in single-crystal measurements [33], and was not seen earlier [34] or in our polycrystalline samples, possibly due to strains.

The CDW distortion (\mathbf{R}_{CDW}) between the α -U and α_2 -U phases primarily involves motion of U atoms along the a -axis. Consistent with earlier work [21], a double-well energy potential with minima at the CDW distortion amplitude ($|\mathbf{R}_{\text{CDW}}|$) confirms this distortion (Supplemental Material, Fig. S2 [35]). Extended x-ray absorption fine structure spectroscopy [66] found $|\mathbf{R}_{\text{CDW}}|$ to be quite small (~ 0.1 Å). Similar to the analysis of Ref. [30], we calculated the probability distribution $P(x)$ of U atoms from the AIMD displacement trajectories, and confirmed both the amplitude and direction of \mathbf{R}_{CDW} [Figs. 1(a) and 1(c)]. As shown in Supplemental Material, Figs. S1a and S1b, q_y and q_z lock in to values of $1/6$ and $5/27$ r.l.u., respectively, on cooling below $T < T_{\alpha_{23}} \sim 22$ K (α_3 -U phase), and lead to a square modulated $2\text{-}q$ state [27] (see Supplemental Material, Note B). A corresponding weak peak is observed in C_p measurements. For the remainder of this Letter, we will limit discussion to the α -U and α_2 -U phases that are relevant to the electronic instability, CDW formation, and Kohn anomalies. We note that all units in the Letter correspond to the notation for the α -U phase.

Multiple Kohn anomalies at the CDW wave vector.—First, we focus on experimental and theoretical evidence of multiple Kohn anomalies at \mathbf{q}_{CDW} . The simulation details are given in the Methods section of the Supplemental Material [35]. Phonon dispersions of α -U within the harmonic approximation using the finite-displacement approach in the $(H, 0, L)$ reciprocal lattice plane are shown in Fig. 2(a). We highlight the Kohn anomaly in three of the branches by white arrows in Figs. 2(b)–2(d). Notably, as illustrated in Supplemental Material Figs. S4 and S5a, multiple Kohn anomalies at \mathbf{q}_{CDW} are also visible in our finite temperature (300 K) and density functional perturbation theory simulations, and are not artifacts of the finite-displacement approach. We discuss below the presence of the Kohn anomaly in individual phonon branches.

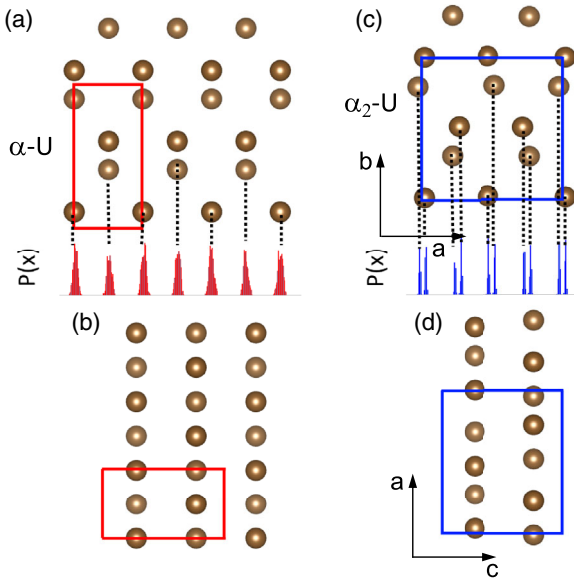


FIG. 1. (a),(b) The orthorhombic lattice structure of α -U above $T_{\text{CDW}} \sim 43$ K in the (a) a - b and (b) a - c planes. Red rectangle denotes the conventional unit cell. The bottom of (a) shows the spatial probability distribution $P(x)$ of U atoms along the a axis obtained from AIMD simulations at 300 K. (c),(d) Same as (a) and (b) but for the α_2 -U phase. The blue rectangle denotes the primitive unit cell. The single peak distribution of $P(x)$ splits into two distinct peaks separated by ~ 0.1 Å below T_{CDW} .

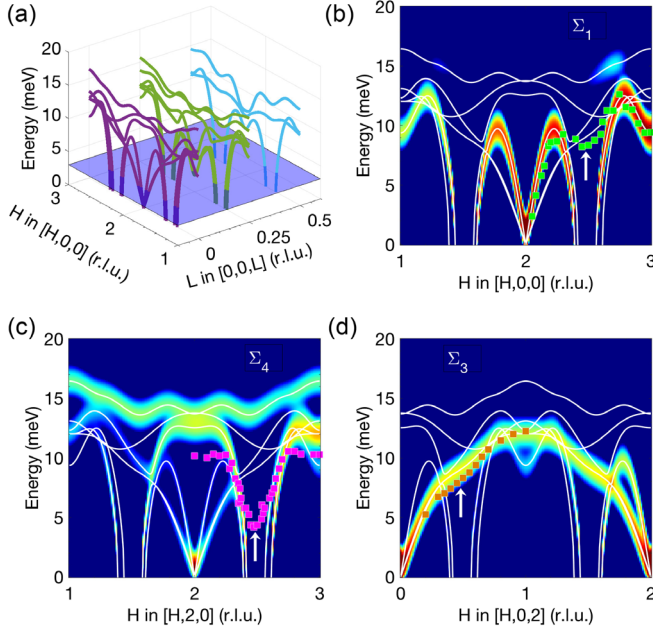


FIG. 2. (a) Phonon dispersions of α -U along the $[H, 0, 0]$ for $L = 0, 0.25$, and 0.5 r.l.u. A constant energy slice at 3 meV in the $(H, 0, L)$ plane is shown by purple color. (b) A comparison of the phonon dispersions along $[H, 0, 0]$ with INS measurements at 300 K (green markers [20]). The dispersions are overplotted with $\chi''_L(\mathbf{Q}, E)$, which selectively highlights the Σ_1 phonon branch (bright red color). The white arrow marks the Kohn anomaly in the phonon dispersion at $H = 2.5$. Color bar is on a logarithmic scale and spans five decades. (c),(d) Same as (b), but for the Σ_4 and Σ_3 phonon branches probed along $[H, 2, 0]$ and $[H, 0, 2]$, respectively. Experimental data [20] are presented with magenta and orange markers.

In Fig. 2(a), we find the two longitudinal phonon branches of acoustic and optic character [LA (Σ_1) and LO (Σ_4)] drop to zero energy and become imaginary near $H = 2.5$ and 1.5 r.l.u. for all L indexes, indicating unstable branches. The instability of the Σ_1 and Σ_4 branches can be explained by the fact that a longitudinal polarization significantly modulates the electron density as opposed to a transverse polarization [4], which cannot be captured within the harmonic approximation. Indeed, as shown in Supplemental Material, Fig. S4 [35], after including coupling between atomic vibrations and electronic states, both branches become stable in anharmonic simulations at 300 K. Figure 2(b) compares $\chi''_L(\mathbf{Q}, E)$ along $[H, 0, 0]$ selectively probing the Σ_1 branch with previous inelastic neutron scattering (INS) measurements of the same branch (green markers, Ref. [20]), illustrating a good agreement except near $H = 2.5$. The Kohn anomaly at $H = 2.5$ is marked by a white arrow. Similarly, a more pronounced Kohn anomaly in the Σ_4 branch is visible along $[H, 2, 0]$ at $H = 2.5$ [Fig. 2(c)]. Notably, the phonon eigenvectors of the Σ_4 branch at $H = 2.5$ overlap with the CDW distortion (Supplemental Material, Figs. S2d and S2e), and phonon

energy $E_{H=2.5}^{\Sigma_4}$ approaches zero at T_{CDW} [27], which allows long-range CDW order to manifest.

In contrast to the marked effect on the Σ_1 and Σ_4 branches, the relatively weak modulation of electron density by the transversely polarized branches is expected to be notable but less pronounced. Figure 2(d) compares $\chi''_L(\mathbf{Q}, E)$ along $[H, 0, 2]$ with INS measurements of the transverse acoustic (Σ_3) branch [20]. Both simulations and measurements show a Kohn anomaly at $H = 0.5$, marked by the white arrow. Importantly, as shown in Supplemental Material, Figs. S5b–S5g [35], we also find peaks (or kinks) in the phonon linewidths Γ_{LW} for multiple branches at \mathbf{q}_{CDW} , as opposed to a peak (or kink) for one of the phonon branches in the *wave-vector-dependent* EPI [8,9,11,12] (see Supplemental Material, Note C, for details). Experimental and theoretical evidence thus allows us to conclude the Kohn anomaly appears in multiple phonon branches at \mathbf{q}_{CDW} .

Here, we emphasize the Kohn anomaly is delocalized in the reciprocal lattice. Indeed it is the 1D response that allows for unambiguous evidence of Kohn anomalies, in particular for transverse branches, as integration over a finite volume (because of finite \mathbf{Q} resolution in experiments) does not smear out weak features. We affirm the 1D response of the anomalies in Supplemental Material, Note D [35]. The origin of multiple Kohn anomalies and 1D response lies in the incipient electronic instability of the α -U phase and *ridgeline* feature in $\text{Re}\{\chi_0(\mathbf{q})\}$, as we discuss below.

Fermi surface topology and Lindhard susceptibility.—As described earlier, electronic instability is governed by $\chi_0(\mathbf{q}, \omega)$, which in turn is obtained from the Fermi surface topology and the electron bands near the Fermi energy (E_F). Electronic band structure of the α -U phase near E_F is shown in Supplemental Material, Figs. S9 and S11 [35], and agrees well with angular-resolved photoemission spectroscopy measurements [23] and simulations of Xie *et al.* [25]. A comparison of the electronic density of states with various spectroscopy measurements of valence and conduction bands (Supplemental Material, Fig. S15) further confirms that experimental features are reliably reproduced. Six electron bands cross E_F . The Fermi surface topology of two bands is illustrated in Figs. 3(a) and 3(b). The remaining four bands are shown in Supplemental Material, Figs. S16c–S16f. As one can see, the Fermi surface has complex 3D features, and the FSN wave vector is hard to decipher immediately. Hence, to locate the FSN wave vector, we evaluated $\text{Im}\{\chi_0(\mathbf{q})\}$ by restricting band energy, i.e., $\epsilon_{\mathbf{k}} = \epsilon_{\mathbf{k}+\mathbf{q}} = E_F$ and searched for divergent peak(s). As shown in Fig. 3(d), $\text{Im}\{\chi_0(\mathbf{q})\}$ is divergent at the zone center, i.e., indices $(0,0,0)$, $(0,1,0)$, $(1,0,0)$, and $(1,1,0)$. Moreover, a broad hump is visible near $H = 0.5$ r.l.u. (marked by a pink ellipse). Thus, our simulations of $\text{Im}\{\chi_0(\mathbf{q})\}$ show divergent behavior at the zone center but find no evidence of finite length FSN wave vector(s).

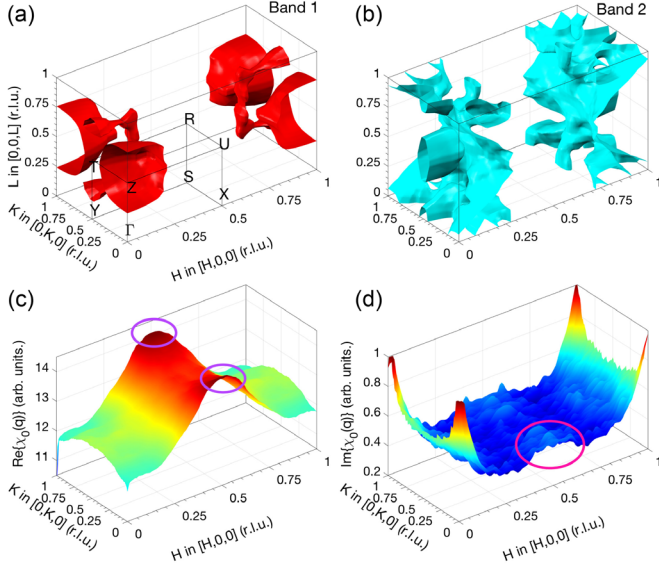


FIG. 3. (a),(b) Reconstruction of the Fermi surface in 3D from the two bands that cross E_F . Separate plots of the Fermi surface from different bands are for ease of visualizing the complex topological features. High-symmetry k points are denoted within (a). (c) $\text{Re}\{\chi_0(\mathbf{q})\}$ and (d) $\text{Im}\{\chi_0(\mathbf{q})\}$ in the $(H, K, 0)$ reciprocal lattice plane. The color scale corresponds to the z -axis coordinates.

Absence of the FSN wave vector in $\text{Im}\{\chi_0(\mathbf{q})\}$ does not imply electronic stability, as instability is governed by $\text{Re}\{\chi_0(\mathbf{q})\}$ [5,6]. The $\text{Re}\{\chi_0(\mathbf{q})\}$ includes contributions from bands above and below E_F as opposed to only contribution from bands at E_F for $\text{Im}\{\chi_0(\mathbf{q})\}$ [5]. Figure 3(c) shows the $\text{Re}\{\chi_0(\mathbf{q})\}$ in the $(H, K, 0)$ plane. As we can observe, $\text{Re}\{\chi_0(\mathbf{q})\}$ is divergent at the reciprocal indices $(0.5, 0, 0)$ and $(0.5, 1, 0)$ (marked by purple ellipses) and the wave vector corresponds to the q_x component of the measured \mathbf{q}_{CDW} . Importantly, we find that $\text{Re}\{\chi_0(\mathbf{q})\}$ has a ridgeline feature that extends along the K index with maxima at $H = 0.5$ r.l.u. Examination of $\text{Re}\{\chi_0(\mathbf{q})\}$ for various values of the L index led to the same ridgeline feature (Supplemental Material, Figs. S20a–S20c [35]), thus emphasizing the (quasi-)1D response of the $\text{Re}\{\chi_0(\mathbf{q})\}$ in the entire reciprocal lattice. To confirm the robustness of the 1D response, we repeated the simulations by shifting E_F as much as 50 meV, and further calculated $\text{Re}\{\chi_0(\mathbf{q}, \omega)\}$ including external perturbations at a given frequency $\omega = 15$ meV (i.e., perturbations from phonons). In both cases, as shown in Supplemental Material, Figs. S21a–S21c and S22a–S22c, we found a 1D response of $\text{Re}\{\chi_0(\mathbf{q})\}$. On the other hand, since $\text{Im}\{\chi_0(\mathbf{q})\}$ includes contributions from the bands at E_F only, for both cases, $\text{Im}\{\chi_0(\mathbf{q})\}$ has different topology, as expected (Supplemental Material, Figs. S21d–S21f and S22d–S22f). This intriguing 1D behavior of $\text{Re}\{\chi_0(\mathbf{q})\}$ prompted us to probe its emergence from the electronic band structure.

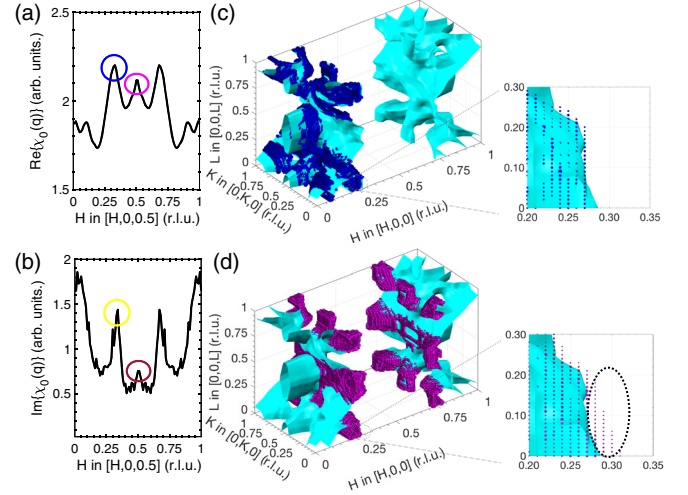


FIG. 4. (a) $\text{Re}\{\chi_0(\mathbf{q})\}$ along $[H, 0, 0.5]$ (integrated over the K axis) showing peaks at $H = 0.34$ and 0.5 r.l.u., marked by blue and magenta ellipses. (b) Same as (a) but for $\text{Im}\{\chi_0(\mathbf{q})\}$ with peaks marked by yellow and maroon ellipses. (c) Contribution of k points from the entire 3D reciprocal lattice to the peak (blue ellipse) in $\text{Re}\{\chi_0(\mathbf{q})\}$. From the entire reciprocal lattice, only the k points lying on or close to the Fermi surface of band 2 contribute; hence, they are overplotted on the Fermi surface for visualization. k points that contribute up to 10% of the maximum value are displayed, with marker size indicating the relative contribution. The enlarged view is a 2D projection in $(H, K, 0)$ plane. (d) Same as (c) but for the peak at $H = 0.5$ r.l.u. in the $\text{Re}\{\chi_0(\mathbf{q})\}$ marked by magenta ellipse. In the enlarged view, k points as far as 0.03 r.l.u. away from the Fermi surface contribute to $\text{Re}\{\chi_0(\mathbf{q})\}$ (black dotted ellipse).

Quantitative analysis of FSN and hidden nesting.—From the outset, we mention that robustness of the 1D response of $\text{Re}\{\chi_0(\mathbf{q})\}$ against the shift in E_F suggested a role of the Fermi surface velocity (v_F), which in favorable conditions (i.e., $v_{F,\mathbf{k}} \simeq -v_{F,\mathbf{k}+\mathbf{q}}$) allows nearby electronic states ($\epsilon_{\mathbf{k}} + v_{F,\mathbf{k}}\delta k$ and $\epsilon_{\mathbf{k}+\mathbf{q}} - v_{F,\mathbf{k}+\mathbf{q}}\delta k$) present above and below the E_F to nest. This form of “hidden nesting” was proposed by Johannes and Mazin for CeTe_3 [5]. We examine one representative slice $[(H, K, 0.5)]$ from the Fermi surface of band 2 [Fig. 3(b)] to investigate if hidden nesting could be the governing mechanism here.

Figure S23a in Supplemental Material shows constant energy contours of band 2 across E_F [35]. Near flat contours along the K index at E_F suggest the possibility of FSN for $\mathbf{q} = (0.5, 0, 0)$ (marked by a purple arrow). However, $\text{Im}\{\chi_0(\mathbf{q})\}$, as shown in Fig. 4(b), indicates otherwise, and only a small peak signifying weak FSN is evident at $H = 0.5$ (maroon ellipse). But, not so apparent on visual inspection, we observe a strong FSN at $H = 0.34$ r.l.u. (yellow ellipse). The corresponding $\text{Re}\{\chi_0(\mathbf{q})\}$ is plotted in Fig. 4(a) and shows pronounced peaks at both $H = 0.34$ and 0.5 r.l.u. (blue and magenta ellipses).

First, we investigate how different k points of the entire reciprocal lattice contribute to the peak at $H = 0.34$.

Figure 4(c) shows the contribution to the peak in $\text{Re}\{\chi_0(\mathbf{q})\}$. The contribution to the peak in $\text{Im}\{\chi_0(\mathbf{q})\}$ is shown in Supplemental Material, Fig. S23e [35]. One observation is apparent—all the contributing k points for both $\text{Re}\{\chi_0(\mathbf{q})\}$ and $\text{Im}\{\chi_0(\mathbf{q})\}$ lie on the Fermi surface of band 2, which we have overplotted for visualization. We note that translation by $\mathbf{q} = (0.34, 0, 0)$ breaks the translational symmetry; hence only one half of the Fermi surface contributes. Since the peak at $H = 0.34$ appears both in the $\text{Re}\{\chi_0(\mathbf{q})\}$ and $\text{Im}\{\chi_0(\mathbf{q})\}$, and originates entirely from FSN (only k points on the Fermi surface contribute), it thus represents a textbook picture of a Peierls instability [1,2]. However, as we considered only one slice among many, this instability is not strong enough to drive the entire lattice response.

Next we focus on the peak at $H = 0.5$. Figure 4(d) shows the contribution to the peak in $\text{Re}\{\chi_0(\mathbf{q})\}$. The contribution to the peak in $\text{Im}\{\chi_0(\mathbf{q})\}$ is shown in Supplemental Material, Fig. S23g [35]. Here translational symmetry is preserved. As we can observe from Supplemental Material, Fig. S23g, few k points contribute to the peak in $\text{Im}\{\chi_0(\mathbf{q})\}$, consistent with a relatively small peak seen in Fig. 4(b). Strikingly, a significantly large number of k points contribute to $\text{Re}\{\chi_0(\mathbf{q})\}$, and even parts of the Fermi surface not contributing to the $\text{Im}\{\chi_0(\mathbf{q})\}$ now have a finite contribution [Fig. 4(d)]. We also notice that a large number of k points as far as 0.03 r.l.u. from the Fermi surface contribute to $\text{Re}\{\chi_0(\mathbf{q})\}$, as highlighted by a dotted ellipse in the enlarged view. This is facilitated by v_F of bands that allow nearby electronic states above and below E_F to nest, as discussed earlier. These observations allow us to conclude that the peak in $\text{Re}\{\chi_0(\mathbf{q})\}$ at $H = 0.5$ originates from both FSN and hidden nesting. Whangbo *et al.* [67] showed that for low-dimensional metals, the signatures of hidden nesting are also etched in the avoided band crossings at E_F . Figure S19 in Supplemental Material shows such a scenario for the same $(H, K, 0.5)$ plane, and using a representative model of two bands illustrates the fragility of the FSN due to the avoided band crossing and its manifestation as hidden nesting.

Here we took the $(H, K, 0.5)$ plane from band 2 as a representative slice. We performed a similar analysis for the entire reciprocal lattice. We find that several pairs of bands (1–3, 1–4, 2–2, 2–3, 2–4, and 3–3), contribute almost equally to the ridgelike feature in the $\text{Re}\{\chi_0(\mathbf{q})\}$ shown in Fig. 3(c). Other remaining pairwise contributions are negligible (i.e., pair of bands 1–4, 1–5, 1–6, ...). For example, the contribution from a pair of bands 2–3 [significant contribution to $\text{Re}\{\chi_0(\mathbf{q})\}$] and 6–6 (negligible contribution) is shown in Supplemental Material, Figs. S24 and S26 [35], respectively. This ridgelike feature, which extends along both the K and L indices, is indeed responsible for the (quasi-)1D response of $\chi_L''(\mathbf{Q}, E)$ and the Kohn anomaly in multiple phonon branches at \mathbf{q}_{CDW} (Fig. 2), as we describe below.

The emergence of Kohn anomalies from the ridgelike feature in $\text{Re}\{\chi_0(\mathbf{q})\}$ has its foundation in the seminal work of Kohn [7]. Kohn showed that for a 3D free-electron gas, the divergence of the derivative of $F(\mathbf{q})$ at $|\mathbf{q}| = 2k_F$ alters the restoring forces (see Supplemental Material, Fig. S27 [35]), and anomalies appear in phonon dispersions at the same \mathbf{q} . Physically, $F(\mathbf{q})$ relates the induced electronic charge density to the embedded charge distribution [7] or equivalently induced potential energy (PE) to total PE [4]. Since the force is a derivative of PE, the force modulation is governed by a derivative of $F(\mathbf{q})$ (which is proportional to $\text{Re}\{\chi_0(\mathbf{q})\}/|\mathbf{q}|^2$) [7]. In α -U, the ridgelike feature in $\text{Re}\{\chi_0(\mathbf{q})\}$ at $H = 0.5$ r.l.u. $\forall K$ and L indices allows the strong modulation of restoring forces between atoms and consequently leads to the Kohn anomaly in multiple phonon branches.

In summary, using a combined experimental and simulation approach, we showed multiple Kohn anomalies and elucidated on their emergence in α -U. We unraveled the hidden nesting of the electronic states, enabled by avoided band crossing and favorable v_F , and found it to be prevalent. This hidden nesting in concert with the FSN induces the ridgelike feature in $\text{Re}\{\chi_0(\mathbf{q})\}$, which in turn due to strong EPI leads to multiple Kohn anomalies at \mathbf{q}_{CDW} . This coupled FSN and hidden nesting scenario is general and could explain CDW transition and the Kohn anomaly in Weyl semimetals [68,69] where linearly dispersing electron bands from two Weyl nodes can nest. Our study opens avenues to understand the coupling of CDW, Kohn anomalies, and superconductivity in α -U [27,31], and extend the same ideas for unraveling their competition in transition metal dichalcogenides [70], heavy-fermion superconductors [71,72], and high-temperature superconductors [73–78].

A. P. R. acknowledges the financial support from IRCC-IITB. N. B. and D. B. thank the financial support from BRNS–DAE under Project No. 58/14/30/2019-BRNS/11117, and MHRD-STARs under Project No. STARs/APR2019/PS/345/FS. We acknowledge the use of the SPACETIME-II supercomputing facility at IITB and ANUPAM supercomputing facility at BARC.

*dipanshu@iitb.ac.in

- [1] R. Peierls, *Quantum Theory of Solids* (Oxford University Press, New York, 1955).
- [2] R. Peierls, *More Surprises in Theoretical Physics* (Princeton University Press, Princeton, NJ, 1991).
- [3] G. Grüner, *Density Waves in Solids* (Addison-Wesley, Reading, MA, 1994).
- [4] M. Dressel and G. Gruner, *Electrodynamics of Solids: Optical Properties of Electrons in Matter* (Cambridge University Press, Cambridge, England, 2002).
- [5] M. D. Johannes and I. I. Mazin, *Phys. Rev. B* **77**, 165135 (2008).
- [6] X. Zhu, Y. Cao, J. Zhang, E. Plummer, and J. Guo, *Proc. Natl. Acad. Sci. U.S.A.* **112**, 2367 (2015).

- [7] W. Kohn, *Phys. Rev. Lett.* **2**, 393 (1959).
- [8] F. Weber, S. Rosenkranz, J.-P. Castellán, R. Osborn, R. Hott, R. Heid, K.-P. Bohnen, T. Egami, A. H. Said, and D. Reznik, *Phys. Rev. Lett.* **107**, 107403 (2011).
- [9] F. Weber, R. Hott, R. Heid, K.-P. Bohnen, S. Rosenkranz, J.-P. Castellán, R. Osborn, A. H. Said, B. M. Leu, and D. Reznik, *Phys. Rev. B* **87**, 245111 (2013).
- [10] C. J. Arguello, S. P. Chockalingam, E. P. Rosenthal, L. Zhao, C. Gutiérrez, J. H. Kang, W. C. Chung, R. M. Fernandes, S. Jia, A. J. Millis, R. J. Cava, and A. N. Pasupathy, *Phys. Rev. B* **89**, 235115 (2014).
- [11] M. Maschek, S. Rosenkranz, R. Heid, A. H. Said, P. Giraldo-Gallo, I. R. Fisher, and F. Weber, *Phys. Rev. B* **91**, 235146 (2015).
- [12] M. Maschek, D. A. Zocco, S. Rosenkranz, R. Heid, A. H. Said, A. Alatas, P. Walmsley, I. R. Fisher, and F. Weber, *Phys. Rev. B* **98**, 094304 (2018).
- [13] S.-K. Chan and V. Heine, *J. Phys. F* **3**, 795 (1973).
- [14] M. Calandra, I. I. Mazin, and F. Mauri, *Phys. Rev. B* **80**, 241108(R) (2009).
- [15] H.-M. Eiter, M. Lavagnini, R. Hackl, E. A. Nowadnick, A. F. Kemper, T. P. Devereaux, J.-H. Chu, J. G. Analytis, I. R. Fisher, and L. Degiorgi, *Proc. Natl. Acad. Sci. U.S.A.* **110**, 64 (2013).
- [16] G. Grimvall, *The Electron-Phonon Interaction in Metals* (North-Holland, Amsterdam, 1981).
- [17] F. Giustino, *Rev. Mod. Phys.* **89**, 015003 (2017).
- [18] K.-P. Bohnen, R. Heid, H. J. Liu, and C. T. Chan, *Phys. Rev. Lett.* **93**, 245501 (2004).
- [19] M. Hoesch, A. Bosak, D. Chernyshov, H. Berger, and M. Krisch, *Phys. Rev. Lett.* **102**, 086402 (2009).
- [20] W. P. Crummett, H. G. Smith, R. M. Nicklow, and N. Wakabayashi, *Phys. Rev. B* **19**, 6028 (1979).
- [21] L. Fast, O. Eriksson, B. Johansson, J. M. Wills, G. Straub, H. Roeder, and L. Nordström, *Phys. Rev. Lett.* **81**, 2978 (1998).
- [22] C. P. Opeil, R. K. Schulze, M. E. Manley, J. C. Lashley, W. L. Hults, R. J. Hanrahan, Jr, J. L. Smith, B. Mihaila, K. B. Blagoev, R. C. Albers, and P. B. Littlewood, *Phys. Rev. B* **73**, 165109 (2006).
- [23] C. P. Opeil, R. K. Schulze, H. M. Volz, J. C. Lashley, M. E. Manley, W. L. Hults, R. J. Hanrahan, Jr, J. L. Smith, B. Mihaila, K. B. Blagoev, R. C. Albers, and P. B. Littlewood, *Phys. Rev. B* **75**, 045120 (2007).
- [24] D. Graf, R. Stillwell, T. P. Murphy, J.-H. Park, M. Kano, E. C. Palm, P. Schlottmann, J. Bourg, K. N. Collar, J. Cooley, and J. Lashley, J. Willit, and S. W. Tozer, *Phys. Rev. B* **80**, 241101 (2009).
- [25] W. Xie, W. Xiong, C. A. Marianetti, and D. Morgan, *Phys. Rev. B* **88**, 235128 (2013).
- [26] Y. Yamada, *Phys. Rev. B* **47**, 5614 (1993).
- [27] G. Lander, E. Fisher, and S. Bader, *Adv. Phys.* **43**, 1 (1994).
- [28] M. E. Manley, B. Fultz, R. J. McQueeney, C. M. Brown, W. L. Hults, J. L. Smith, D. J. Thoma, R. Osborn, and J. L. Robertson, *Phys. Rev. Lett.* **86**, 3076 (2001).
- [29] M. E. Manley, M. Yethiraj, H. Sinn, H. M. Volz, A. Alatas, J. C. Lashley, W. L. Hults, G. H. Lander, and J. L. Smith, *Phys. Rev. Lett.* **96**, 125501 (2006).
- [30] J. Bouchet and F. Bottin, *Phys. Rev. B* **92**, 174108 (2015).
- [31] S. Raymond, J. Bouchet, G. H. Lander, M. Le Tacon, G. Garbarino, M. Hoesch, J.-P. Rueff, M. Krisch, J. C. Lashley, R. K. Schulze, and R. C. Albers, *Phys. Rev. Lett.* **107**, 136401 (2011).
- [32] Z. E. Brubaker, S. Ran, A. H. Said, M. E. Manley, P. Söderlind, D. Rosas, Y. Idell, R. J. Zieve, N. P. Butch, and J. R. Jeffries, *Phys. Rev. B* **100**, 094311 (2019).
- [33] J. Crangle and J. Temporal, *J. Phys. F* **3**, 1097 (1973).
- [34] R. Hall and M. Mortimer, *J. Low Temp. Phys.* **27**, 313 (1977).
- [35] See Supplemental Material at <http://link.aps.org/supplemental/10.1103/PhysRevLett.126.096401> for Methods, Notes A–D, and Figs. S1–S27, which includes Refs. [36–63].
- [36] D. Wallace, *Thermodynamics of Crystals* (John Wiley & Sons Inc., New York, 1972).
- [37] B. Fultz, *Prog. Mater. Sci.* **55**, 247 (2010).
- [38] G. Kresse and J. Hafner, *Phys. Rev. B* **47**, 558 (1993).
- [39] G. Kresse and J. Furthmüller, *Phys. Rev. B* **54**, 11169 (1996).
- [40] G. Kresse and J. Furthmüller, *Comput. Mater. Sci.* **6**, 15 (1996).
- [41] J. P. Perdew, K. Burke, and M. Ernzerhof, *Phys. Rev. Lett.* **77**, 3865 (1996).
- [42] S. L. Dudarev, G. A. Botton, S. Y. Savrasov, C. J. Humphreys, and A. P. Sutton, *Phys. Rev. B* **57**, 1505 (1998).
- [43] A. N. Chantis, R. C. Albers, M. D. Jones, M. van Schilfgaarde, and T. Kotani, *Phys. Rev. B* **78**, 081101(R) (2008).
- [44] J.-W. Yang, T. Gao, B.-Q. Liu, G.-A. Sun, and B. Chen, *Phys. Status Solidi B* **252**, 521 (2015).
- [45] S. Zhou, R. Jacobs, W. Xie, E. Tea, C. Hin, and D. Morgan, *Phys. Rev. Mater.* **2**, 083401 (2018).
- [46] F. Bottin, J. Bieder, and J. Bouchet, *Comput. Phys. Commun.* **254**, 107301 (2020).
- [47] C. Barrett, M. Mueller, and R. Hitterman, *Phys. Rev.* **129**, 625 (1963).
- [48] A. Togo and I. Tanaka, *Scr. Mater.* **108**, 1 (2015).
- [49] Y. Baer and J. K. Lang, *Phys. Rev. B* **21**, 2060 (1980).
- [50] X. Yang and P. S. Riseborough, *Phys. Rev. B* **82**, 094303 (2010).
- [51] P. B. Allen, T. Berlijn, D. A. Casavant, and J. M. Soler, *Phys. Rev. B* **87**, 085322 (2013).
- [52] U. Herath, P. Tavazde, X. He, E. Bousquet, S. Singh, F. Muoz, and A. H. Romero, *Comput. Phys. Commun.* **251**, 107080 (2020).
- [53] O. Hellman, I. A. Abrikosov, and S. I. Simak, *Phys. Rev. B* **84**, 180301(R) (2011).
- [54] O. Hellman and I. A. Abrikosov, *Phys. Rev. B* **88**, 144301 (2013).
- [55] O. Hellman, P. Steneteg, I. A. Abrikosov, and S. I. Simak, *Phys. Rev. B* **87**, 104111 (2013).
- [56] C. H. Chen and G. H. Lander, *Phys. Rev. Lett.* **57**, 110 (1986).
- [57] H. G. Smith and G. H. Lander, *Phys. Rev. B* **30**, 5407 (1984).
- [58] S. Poncé, E. R. Margine, C. Verdi, and F. Giustino, *Comput. Phys. Commun.* **209**, 116 (2016).
- [59] F. Giustino, M. L. Cohen, and S. G. Louie, *Phys. Rev. B* **76**, 165108 (2007).
- [60] P. Giannozzi *et al.*, *J. Phys. Condens. Matter* **21**, 395502 (2009).

- [61] P. Giannozzi *et al.*, *J. Phys. Condens. Matter* **29**, 465901 (2017).
- [62] M. Brodsky, N. Griffin, and M. Odie, *J. Appl. Phys.* **40**, 895 (1969).
- [63] S. Aarj, R. H. Flora, and E. E. Anderson, *J. Nucl. Mater.* **37**, 89 (1970).
- [64] J.-C. Marmeggi, G. H. Lander, S. Van Smaalen, T. Brückel, and C. M. E. Zeyen, *Phys. Rev. B* **42**, 9365 (1990).
- [65] G. Grübel, J. D. Axe, D. Gibbs, G. H. Lander, J. C. Marmeggi, and T. Brückel, *Phys. Rev. B* **43**, 8803 (1991).
- [66] E. J. Nelson, P. G. Allen, K. J. M. Blobaum, M. A. Wall, and C. H. Booth, *Phys. Rev. B* **71**, 184113 (2005).
- [67] M.-H. Whangbo, E. Canadell, P. Foury, and J.-P. Pouget, *Science* **252**, 96 (1991).
- [68] J. Gooth, B. Bradlyn, S. Honnali, C. Schindler, N. Kumar, J. Noky, Y. Qi, C. Shekhar, Y. Sun, Z. Wang, B. Bernevig, and C. Felser, *Nature (London)* **575**, 315 (2019).
- [69] T. Nguyen, F. Han, N. Andrejevic, R. Pablo-Pedro, A. Apte, Y. Tsurimaki, Z. Ding, K. Zhang, A. Alatas, E. E. Alp *et al.*, *Phys. Rev. Lett.* **124**, 236401 (2020).
- [70] Y. I. Joe, X. Chen, P. Ghaemi, K. Finkelstein, G. de La Peña, Y. Gan, J. Lee, S. Yuan, J. Geck, G. MacDougall *et al.*, *Nat. Phys.* **10**, 421 (2014).
- [71] P. J. Moll, B. Zeng, L. Balicas, S. Galeski, F. F. Balakirev, E. D. Bauer, and F. Ronning, *Nat. Commun.* **6**, 6663 (2015).
- [72] D. Aoki, K. Ishida, and J. Flouquet, *J. Phys. Soc. Jpn.* **88**, 022001 (2019).
- [73] D. Reznik, L. Pintschovius, M. Ito, S. Iikubo, M. Sato, H. Goka, M. Fujita, K. Yamada, G. Gu, and J. Tranquada, *Nature (London)* **440**, 1170 (2006).
- [74] J. J. Hamlin, D. A. Zocco, T. A. Sayles, M. B. Maple, J.-H. Chu, and I. R. Fisher, *Phys. Rev. Lett.* **102**, 177002 (2009).
- [75] G. Ghiringhelli, M. Le Tacon, M. Minola, S. Blanco-Canosa, C. Mazzoli, N. Brookes, G. De Luca, A. Frano, D. Hawthorn, F. He *et al.*, *Science* **337**, 821 (2012).
- [76] R. Comin, A. Frano, M. M. Yee, Y. Yoshida, H. Eisaki, E. Schierle, E. Weschke, R. Sutarto, F. He, A. Soumyanarayanan *et al.*, *Science* **343**, 390 (2014).
- [77] M. Le Tacon, A. Bosak, S. M. Souliou, G. Dellea, T. Loew, R. Heid, K.-P. Bohnen, G. Ghiringhelli, M. Krisch, and B. Keimer, *Nat. Phys.* **10**, 52 (2014).
- [78] S. Lee, G. De La Peña, Stella X.-L. Sun, M. Mitrano, Y. Fang, H. Jang, J.-S. Lee, C. Eckberg, D. Campbell, J. Collini, J. Paglione, F. M. F. de Groot, and P. Abbamonte, *Phys. Rev. Lett.* **122**, 147601 (2019).